Correct generation of the bound set-down for surface gravity wave groups in laboratory experiments of intermediate to shallow depth

Mortimer, William; Raby, Alison; Antonini, Alessandro; Greaves, Deborah; van den Bremer, Ton S.

DOI
10.1016/j.coastaleng.2022.104121

Publication date
2022

Document Version
Final published version

Published in
Coastal Engineering

Citation (APA)
Mortimer, W., Raby, A., Antonini, A., Greaves, D., & van den Bremer, T. S. (2022). Correct generation of the bound set-down for surface gravity wave groups in laboratory experiments of intermediate to shallow depth. *Coastal Engineering*, *174*, Article 104121. https://doi.org/10.1016/j.coastaleng.2022.104121

Coastal Engineering 174 (2022) 104121

Contents lists available at ScienceDirect

Coastal Engineering

journal homepage: www.elsevier.com/locate/coastaleng

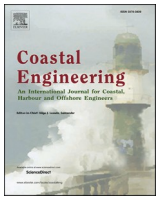

Correct generation of the bound set-down for surface gravity wave groups in laboratory experiments of intermediate to shallow depth

William Mortimer [a,b], Alison Raby [a], Alessandro Antonini [c], Deborah Greaves [a], Ton S. van den Bremer [c,d,*]

[a] Faculty of Science and Engineering, University of Plymouth, Plymouth, PL4 8AA, UK
[b] JBA Consulting Ltd., Newcastle-upon-Tyne, NE1 5JE, UK
[c] Faculty of Civil Engineering and Geosciences, Delft University of Technology, Delft, 2628, CD, the Netherlands
[d] Department of Engineering Science, University of Oxford, Oxford, OX1 3PJ, UK

ARTICLE INFO

Keywords:
Focused wave groups
Second-order wave generation
Harmonic decomposition
Set-down
Error waves

ABSTRACT

Using linear (first-order) wave generation theory in laboratory experiments, leads to significant contamination of the wave field by free non-linear (second-order) error waves, increasingly so at shallower depths. Second-order wave generation theory has previously been established, and so has correct generation of the bound set-down, made up from second-order bound waves in the sub-harmonic part of the spectrum, for bichromatic and irregular wave fields in shallow to intermediate depth. In the present work, different from previous studies, we validate second-order wave theory explicitly for isolated wave groups, which provide a demanding test on the correct generation of sub-harmonic bound waves and the stroke length of the wavemaker. We do so for shallow to intermediate water depth, where some previous attempts at full elimination of sub-harmonic error waves have been hampered by limited paddle stroke. We overcome these limitations by applying second-order wavemaker theory to a piston-type paddle with an extended paddle stroke that can thence generate the bound set-down correctly. We show that sub-harmonic error waves are eliminated by considering wave groups in relative depths k_0d = 0.6–1.1, with important applications in coastal engineering experiments, such as run-up and overtopping.

1. Introduction

Occurrence of wave-induced coastal flooding is expected to increase due to the combined effects of sea level rise (Taherkhani et al., 2020) and more frequent occurrence of large transient waves in the coastal environment (Cattrell et al., 2019; Young and Ribal, 2019). Large transient waves events can pose significant threat to coastal assets, primarily due to their ability to damage and overtop coastal flood defences (see Dawson et al. (2016)). Such waves are highly nonlinear and highly transient, yet they are a key design condition for coastal engineering schemes (Van der Meer et al., 2018) and therefore require accurate estimation by coastal engineers.

Focused wave groups provide an efficient approach to approximate large transient wave events using a compact wave group of select component frequencies. They have been widely used in coastal engineering research (Longuet-Higgins, 1974; Chan and Melville, 1988; Drazen et al., 2008; Tian et al., 2011; Fernández et al., 2014; Antonini et al., 2017; Abroug et al., 2020; Fang et al., 2020) and have been suggested as a design wave in industry-recommended practice (Det Norske Veritas, 2010; ISO:19 901-1:2015).

In general, wave-driven structural responses of interest to coastal engineers are related to the most severe waves of a sea state. Focused wave groups offer the ability to recreate these wave conditions through judicious selection of the underlying energy spectrum, permitting assessment of the associated structural responses in a time efficient and highly repeatable manner (e.g., Borthwick et al. (2006); Hofland et al. (2014)), when compared with irregular wave tests. Focused wave groups are used within a framework known both as NewWave theory (Tromans et al., 1991; Jonathan and Taylor, 1997; Walker and Taylor, 2004; Taylor and Williams, 2004; Borthwick et al., 2006; Whittaker et al., 2016; Chen et al., 2018) and the theory of quasi-determinism (QD) (Boccotti, 1983, 1989, 2000), based on the statistical underpinnings of Lindgren (1970). In this framework, the average shape of an extreme wave crest in a linear random Gaussian sea (i.e., the linear surface

* Corresponding author. Faculty of Civil Engineering and Geosciences, Delft University of Technology, Delft, 2628, CD, the Netherlands.
E-mail address: t.s.vandenbremer@tudelft.nl (T.S. van den Bremer).

https://doi.org/10.1016/j.coastaleng.2022.104121
Received 15 April 2021; Received in revised form 11 March 2022; Accepted 21 March 2022
Available online 30 March 2022

Table 1
Studies that have implemented second-order wave generation.

Authors of study	Method Used	k_0d	Wave types used in study	Validated in freq.	Validated in time	Assessment of agreement between theory and experiments in the time and frequency.
Barthel et al. (1983)		0.6	Bichromatic	✓	✓	Excellent agreement in time. Reasonable agreement in frequency with some under-prediction of magnitude.
Barthel et al. (1983)		1.1	Bichromatic	✓	✓	Partial agreement in time and poor agreement in frequency with significant under-prediction of magnitude.
Barthel et al. (1983)		0.7	Irregular	✓	✓	Excellent agreement in time and frequency.
Barthel et al. (1983)		0.9	Irregular	✓	✓	No improvement in agreement in time and worse agreement in frequency with second-order generation.
Schäffer (1996)	Includes correction of Barthel et al. (1983)	0.6–1.2	Bichromatic	×	✓	Good agreement in time across k_0d range, correcting the results of Barthel et al. (1983) for $k_0d = 1.1$, less good agreement when non-linearity is large. No comparison in frequency.
Schäffer (1996)	Includes correction of Barthel et al. (1983)	0.7 and 0.9	Irregular	×	✓	Excellent agreement in time including cross-correlation analysis. No comparison in frequency.
Van Leeuwen and Klopman (1996)		1.0–1.2	Bichromatic	✓	✓	Good agreement shown in comparison between amplitudes of bound components.
Van Leeuwen and Klopman (1996)		1.0	Irregular	✓	×	Reasonable agreement in frequency with some remaining free waves present probably due to noise, also for broad-banded spectra. No comparison in time.
Boers (1996); Battjes et al. (2004)	Van Leeuwen and Klopman (1996)	0.5–0.9	Irregular	×	×	No validation presented.
Baldock et al. (2000)	Barthel et al. (1983)	1.4–3.4	Bichromatic	✓	✓	Validation of amplitudes only.
Sriram et al. (2015)	Schäffer (1996)	1.5	Isolated groups	×	✓	Excellent agreement in time.
Sriram et al. (2015)	Schäffer (1996)	3.4	Isolated groups	×	×	No validation presented.
Whittaker et al. (2017)	Schäffer (1996)	0.7	Isolated groups	×	×	Limited agreement in time, achieving a reduction of 60% in the sub-harmonic error wave amplitude due to constraints on paddle stroke.
Martins et al. (2021) (GLOBEX)	Van Leeuwen and Klopman (1996)	0.9–1.5	Irregular & bichromatic	×	×	No validation presented.
Present study	Van Leeuwen and Klopman (1996)	0.6–1.1	Isolated groups	✓	✓	Excellent agreement in time and frequency across k_0d range.

elevation follows a Gaussian distribution) can be approximated by the scaled autocorrelation function of the underlying free surface.

Use of focused wave groups in deep-water scenarios is well established, and application in shallower-water scenarios is becoming common. Whittaker et al. (2016) demonstrated that a NewWave/QD group that is corrected for second-order bound waves can reproduce the average shape of the largest wave crests in shallow water ($k_0d < 0.5$). Borthwick et al. (2006); Orszaghova et al. (2014); Whittaker et al. (2017), and Judge et al. (2019) used similar groups to investigate flow kinematics and wave run-up on plane beaches. Hunt (2003); Orszaghova et al. (2014); Hofland et al. (2014), and Antonini et al. (2017) examined wave overtopping and Whittaker et al. (2018) and Chen et al. (2018) wave forcing on inclined to vertical coastal structures and surface-piercing columns. Karmpadakis and Swan (2020) found that when assessing storm-sea time series for the largest (e.g., 1%) wave crests, there is a likelihood that the breaking status of the waves is neglected. Therefore, comparing a focused wave group profile to the average shape of the largest crests could reach an inappropriate conclusion. They found that a focused wave group, specifically in the form of the NewWave/QD framework, provides good approximation of large wave shapes in finite depth. Yet, they note that such wave crest statistics are significantly amplified by high-order nonlinear wave-wave interactions (above second-order), where the nonlinear amplification of wave crests in very steep sea states has poor agreement with the NewWave/QD framework.

Nonlinear free error waves are an inherent product of first-order wave generation (Barthel et al., 1983; Schäffer, 1996). Error waves are widely discussed in literature, where they are also referred to as parasitic or spurious waves (e.g., Hunt (2003); Orszaghova et al. (2014); Aknin and Spinneken (2017); Vyzikas et al. (2018), and Pierella et al. (2021)). They are created through a disparity between bound sub- and super-harmonics present in the wave field and the first-order boundary condition at the wavemaker's face (e.g., Schäffer (1996)). In multi-frequency wave fields, such as focused wave groups, error waves at sub- and super-harmonic frequencies are produced as an instantaneous correction for the absence of bound nonlinearities in the wavemaker displacement. Free error waves satisfy the linear dispersion relation, so freely disperse at a celerity defined by their frequency. Generally, sub-harmonic error waves travel faster than the first-order wave group and are first to arrive at the domain of interest, whereas super-harmonic error waves travel more slowly and trail behind (e.g., Hunt (2003)). Therefore, due to their faster speeds and long wave lengths, sub-harmonic error waves present the most persistent challenge to experimentalists.

Orszaghova et al. (2014) found major discrepancy in run-up and overtopping induced by wave groups due to the presence of sub-harmonic error waves. Their Boussinesq-type numerical model showed sub-harmonic error waves increased run-up by 18–57% and overtopping volumes by 25–83%. Borthwick et al. (2006); Hunt-Raby et al. (2011); Buldakov et al. (2017), and Calvert et al. (2019) also

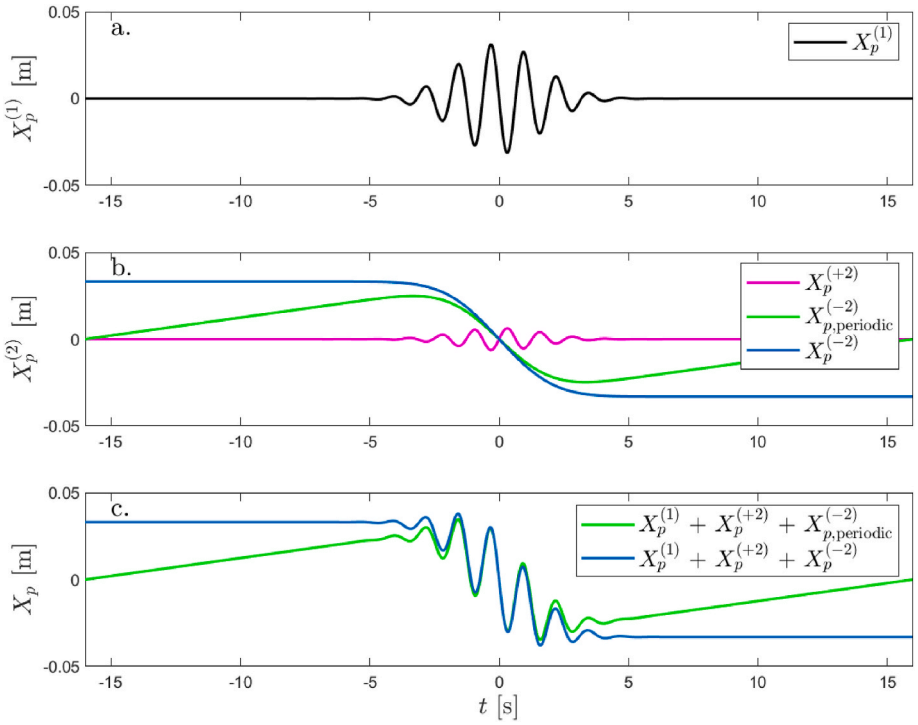

Fig. 1. Example second-order accurate wavemaker displacement time series for a Gaussian group: (a) first-order, (b) second-order, decomposed into super-harmonic $X_p^{(+2)}$, periodic sub-harmonic $X_{p,\text{periodic}}^{(-2)}$ and non-periodic sub-harmonic $X_p^{(-2)}$, and (c) the complete second-order accurate wavemaker displacements.

document how sub-harmonic error waves affect laboratory results. Calvert et al. (2019) notes that in deep-water experiments, sub-harmonic error waves are found to have a negligible affect, so the considerable effort required to mitigate them is often not worthwhile, yet in finite water depth, the effect is much more pronounced and so their mitigation becomes essential.

Second-order wave generation theory has been well established for nearly three decades (Barthel et al., 1983; Schäffer, 1996; Van Leeuwen and Klopman, 1996), and numerous studies have implemented the theory to a varying degree of success. Barthel et al. (1983) provided the first results of second-order correct wave generation based on a broad-banded approach, but did not account for evanescent modes interaction terms in the paddle transfer function. Schäffer (1996) developed the work of Barthel et al. and included correction for evanescent modes; their effect was investigated in Schäffer (1994). Van Leeuwen and Klopman (1996) derived a simpler result for the second-order sub-harmonic paddle signal based on a narrow-bandwidth assumption, making use of the method of multiple scales.

Table 1 compares a selection of experimental studies in which second-order wave generation has been implemented. The table includes the key contributions to the development and validation of (sub-harmonic) second-order wave generation from various studies. The table includes the relative water depth, k_0d, and the wave types used (bichromatic, irregular or isolated groups) in the study. Furthermore, we note whether validation has been carried out in the frequency and/or the time domain. This distinction is important for isolated groups as time-domain comparisons allow a comparison of the amplitude, shape and alignment of the set-down, whereas frequency-domain comparison allow assessment of whether all wave periods are correctly represented, including the longer waves, which may suffer from paddle stroke limitations the most.

Summarising, Barthel et al. (1983) were able to obtain good agreement between the theory they developed and experiments for both bichromatic and irregular waves for shallow water ($k_0d = 0.6$–0.7), but not in intermediate water ($k_0d = 0.9$–1.1). The theory by Barthel et al. (1983) was corrected by Schäffer (1996), who derived a full multi-chromatic theory for wave generation. Schäffer found good agreement for bichromatic and irregular wave fields in both shallow and intermediate water depths ($k_0d = 0.6$–1.2). By considering narrow-banded packets, Van Leeuwen and Klopman (1996) were able to validate their result for both bichromatic and irregular waves in intermediate water depths ($k_0d = 1.0$–1.2). Furthermore, Van Leeuwen and Klopman note that their method is also applicable to large bandwidths in practice despite the theoretical narrow-bandwidth limit their results rely on (a conclusion findings in the present paper will support). Only Sriram et al. (2015) (for their shallowest case) and Whittaker et al. (2017) (partially) have validated second-order wave generation for isolated wave groups, with Sriram et al. (2015) examining wave groups in intermediate to deep water and Whittaker et al. (2017) only achieving a 60% reduction of the sub-harmonic free error wave amplitude in shallow water depths.

Schäffer (1996), builds upon the work of Barthel et al. (1983), and derived a formulation for the complete (i.e., no bandwidth limitations) second-order paddle displacement signals for both piston and pivot-type wavemakers, which is based on a traditional, multi-frequency Stokes--type perturbation expansion. Schäffer's theory dictates that the paddle's (sub-harmonic) backward stroke length increases as k_0d decreases. This means that in shallow water depths, not only is the effect of error waves greater, but also the required paddle sub-harmonic stroke length is greater too. Schäffer presents experimental results in water depths of, $k_0d = 0.6$ up to 1.1.

Herein, we focus on sub-harmonic generation, yet we note for completeness that Spinneken and Swan (2009a,b); Aknin and Spinneken (2017) derived and successfully implemented second-order theory using force-feedback wavemaker control. The complexity of the method meant it is only applicable to mitigating super-harmonic error waves in regular wave fields. Moreover, we do not examine wave absorption. We note that for irregular or long-duration cases absorption is essential and has been successfully implemented.

For isolated focused wave groups, such as those given by the New-Wave/QD framework, the time signal of the wave group corresponds to an infinite repeat period and an infinitesimal frequency discretization,

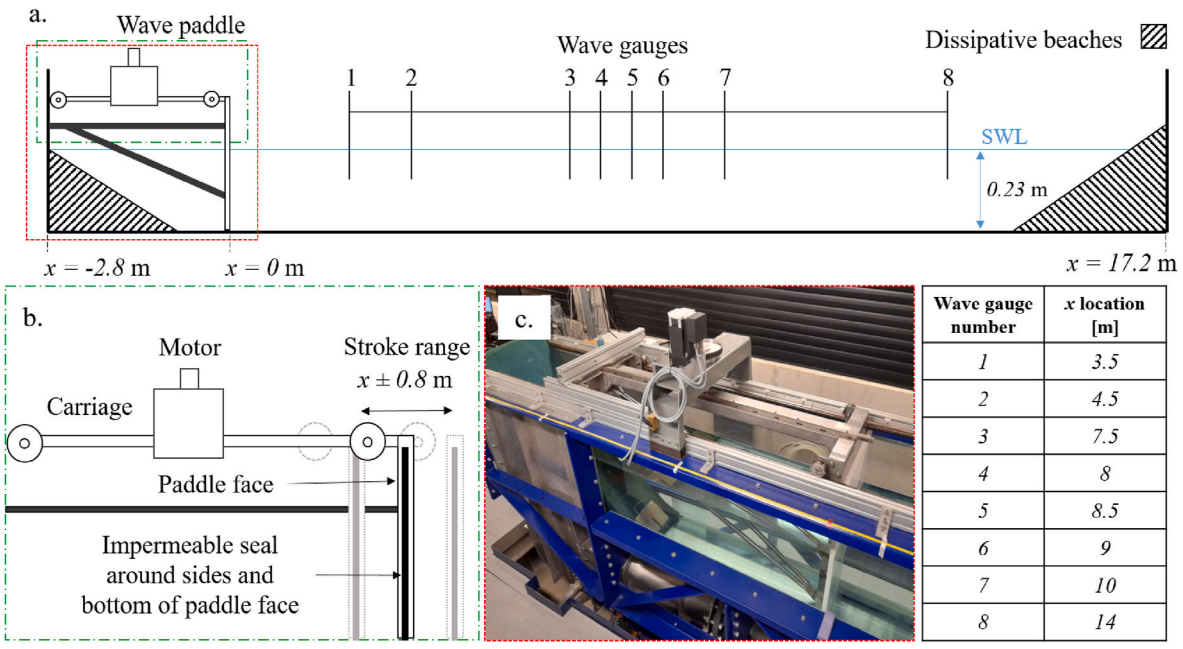

Wave gauge number	x location [m]
1	3.5
2	4.5
3	7.5
4	8
5	8.5
6	9
7	10
8	14

Fig. 2. (a) Experimental set-up: (a) overview of the 20 m-flume with the wave gauge x-locations noted in the table (bottom right), (b) zoomed-in schematic representation of the wavemaker and its operating system, (c) photograph of the wavemaker.

Table 2
Experimental input matrix.

Expt.	f_0 [Hz]	a_0 [m]	σ [m]	$c_{g,0}$ [m/s]	$\Delta X_{p,\text{total}}^{(-2)}$ [m]	$k_0 d$	$\varepsilon = k_0 a_0$	ν
1	0.6	0.034	4.70	1.27	−0.57	0.61	0.09	0.10
2	0.6	0.034	2.51	1.27	−0.31	0.61	0.09	0.19
3	0.6	0.034	1.51	1.27	−0.18	0.61	0.09	0.32
4	0.8	0.024	3.37	1.11	−0.11	0.85	0.09	0.09
5	0.8	0.024	1.80	1.11	−0.07	0.85	0.09	0.17
6	0.8	0.024	1.08	1.11	−0.04	0.85	0.09	0.29
7	1.0	0.040	2.53	0.94	−0.03	1.14	0.20	0.08
8	1.0	0.040	1.35	0.94	−0.02	1.14	0.20	0.16
9	1.0	0.040	0.81	0.94	−0.01	1.14	0.20	0.26

where the signals are constructed from periodic Fourier components, such as in the theory of Schäffer (1996). This means that the resulting paddle displacements in Schäffer (1996) are, in practice (unless an infinite number of Fourier components is used), always periodic, and slow forwards movement is required before and after the first-order group generation. The periodic paddle displacement resembles a saw-tooth displacement profile (displayed in Fig. 1). In the laboratory, relatively long signals (much longer than the wave group itself) need to be created in order for the finite repeat period (as an arbitrary time scale to be chosen by the experimentalist) not to result in additional sub-harmonic energy being created and interfering with the correct generation of the sub-harmonic bound waves.

Finer frequency discretization can be used to mitigate this unwanted response in the sub-harmonic wavemaker displacement. In the narrow-banded theory of Van Leeuwen and Klopman (1996), which makes uses of the method of multiple scales, isolated wave groups with an infinite repeat period are readily obtained in the time domain. Second-order wavemaker theory then encompasses a net (sub-harmonic) backwards movement of the paddle during wave group generation. The sub-harmonic wavemaker signal is readily evaluated in the form of an integral of the (square of the) wave group envelope in the time domain, which is inexpensive to compute.

In this paper, we apply the second-order wave generation theory derived by Van Leeuwen and Klopman (1996) to a prototype, piston-type wavemaker to generate isolated wave groups. The wavemaker has a long stroke length, allowing second-order (sub--harmonic) wave generation to be applied to shallow to intermediate water depths of $k_0 d = 0.6$–1.1. We present surface elevation measurements of a range of focused wave groups, comparing cases with first-order and second-order accurate wave generation. Our work aims to provide a simple methodology that can be employed by coastal engineers in future experimental campaigns concerned with wave-structure interaction studies using focused wave groups or to validate the efficacy of existing wavemakers with built-in second-order generation.

2. Review of the wavemaker theory

We begin by reviewing the second-order wavemaker theory we implement to control our new long-stroke, piston-type wavemaker. A piston-type paddle operates with its paddle face moving horizontally through the entire water column in response to a predetermined displacement time series. This second-order accurate paddle signal is denoted as

$$X_p(t) = X_p^{(1)} + X_p^{(2)}, \tag{1}$$

where the superscript corresponds to the order in steepness. The second-order displacement is the sum of sub and super-harmonic displacements ($X_p^{(2)} = X_p^{(-2)} + X_p^{(+2)}$).

2.1. First-order wave generation $X_p^{(1)}$

The surface elevation of a linearly focused wave group, composed of N frequencies, is given as

$$\eta^{(1)}(x,t) = \sum_{n=1}^{N} a_n \cos\left(k_n(x - x_f) - \omega_n(t - t_f) + \varphi_f\right), \tag{2}$$

where x denotes location in a flume away from the wave generation origin at $x = 0$, t is time, x_f and t_f note the desired spatial and temporal focus locations, a_n is the amplitude, k_n the wavenumber, and ω_n the angular frequency of the nth component. Phasing of the nth component is determined by frequency dependent linear dispersion ($\omega_n^2 = gk_n \tanh(k_n d)$, where d is water depth). The desired shape of the wave

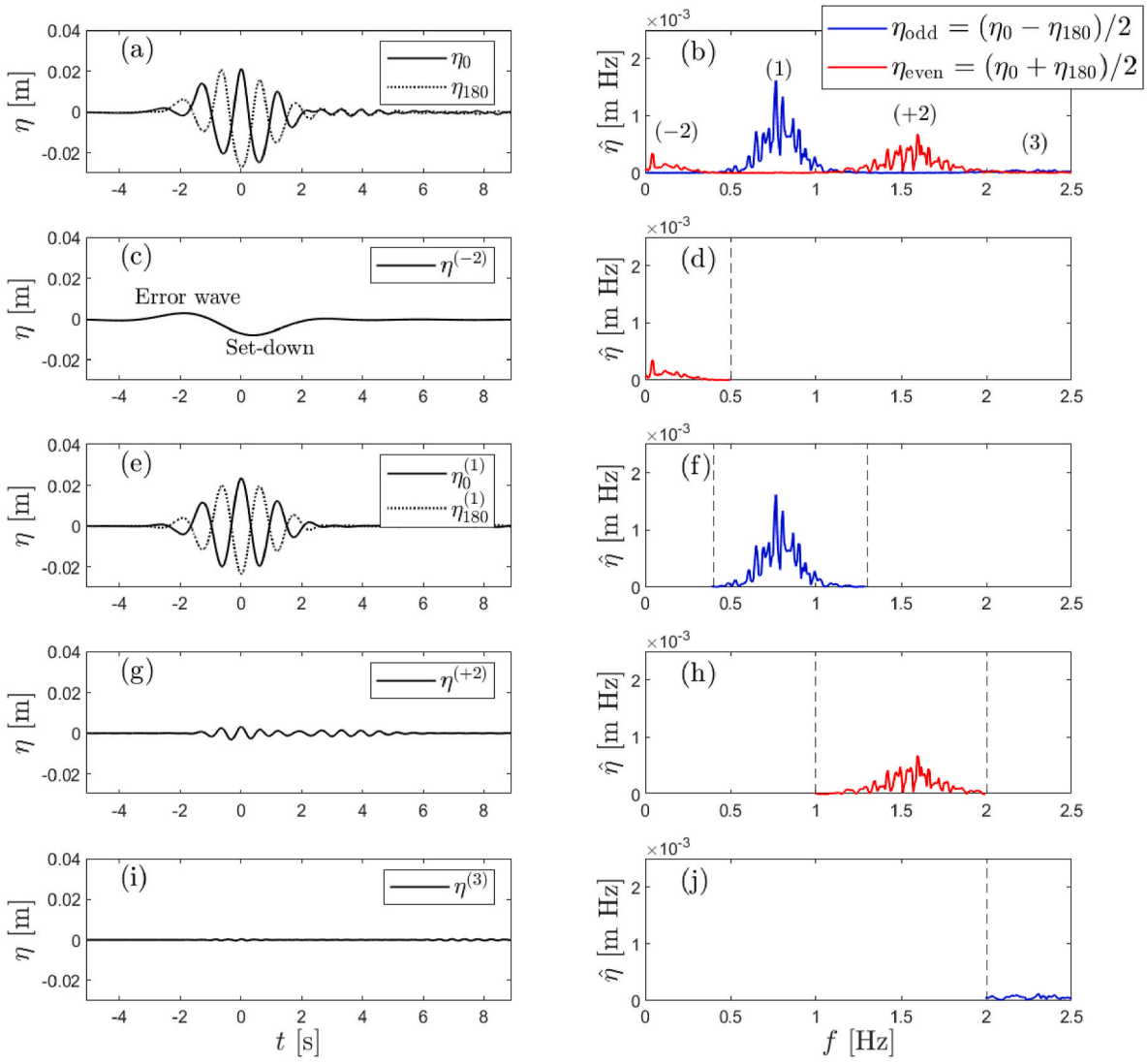

Fig. 3. Illustration of the symmetry-based harmonic separation between crest-focused (η_0) and trough-focused (η_{180}) groups. The left panels (a,c,e,g,i) show surface elevation time series. The right panels (b,d,f,h,j) show corresponding amplitude spectra. Panel a shows two inverted time series, composed of first-order, second-order (sub and super-harmonic) and third-order components. Panel b shows the frequency domain result of two combinations of the inverted groups. The subsequent panels below show individually isolated harmonics in time and frequency domain.

group at focus dictates the phasing of the component waves. A crest-focused group is produced when $\varphi_f = 0°$, a trough-focused group when $\varphi_f = 180°$ and up or down crossings at focus when $\varphi_f = 90°$ or 270°, respectively. The paddle displacement for a first-order wave group is 90° out of phase with the surface elevation field and given as

$$X_p^{(1)} = \sum_{n=1}^{N} a_{p,n} \sin\left(k_n(x - x_f) - \omega_n(t - t_f) + \varphi_f\right), \tag{3}$$

where $a_{p,n}$ is the amplitude of paddle displacement related to a_n through the paddle transfer function. The first-order paddle transfer function for a piston-type wavemaker is given as (e.g., Biésel and Suquet (1951); Ursell et al. (1960); Flick and Guza (1980); Sand and Donslund (1985))

$$\frac{a_n}{a_{p,n}} = k_n d \frac{\tanh(k_n d)}{D_n(k_n d)} \quad \text{with} \quad D_n(k_n d) = \frac{k_n d}{2}\left(\frac{k_n d}{\sinh(k_n d)\cosh(k_n d)} + 1\right). \tag{4}$$

The first-order wave field comprises a progressive wave, matching the intended surface elevation, eq. (2), away from $x = 0$, and evanescent modes, which are products of the disparity between the paddle face's flat geometry and the local depth-varying velocity profile. Evanescent modes decay rapidly away from the paddle, typically becoming negligible at a distance of $x = 3d$ (e.g., Dean and Dalrymple (1991)).

2.2. Second-order wave generation $X_p^{(2)}$

To apply the wavemaker theory of Van Leeuwen and Klopman (1996), we must rewrite eq. (2) using the narrow-bandwidth approximation made in Van Leeuwen and Klopman (1996). To do so, we first express eq. (2) using complex notation

$$\eta^{(1)}(x,t) = \mathrm{Re}\left[\sum_{n=1}^{N} a_n e^{i\left(k_n(x-x_f) - \omega_n(t-t_f) + \varphi_f\right)}\right]. \tag{5}$$

Approximating the linear dispersion relationship as $\omega_n \approx \omega_0 + c_{g,0}(k_n - k_0)$ with $c_{g,0} = \partial\omega/\partial k|_{k_0}$, consistent with the narrow-bandwidth approximation, eq. (5) can be rewritten as

$$\eta^{(1)}(x,t) = \mathrm{Re}\left[A(x - c_{g,0}t)e^{i\left(k_0(x-x_f) - \omega_0(t-t_f) + \varphi_f\right)}\right] \tag{6}$$

with

$$A = \sum_{n=1}^{N} a_n e^{i\left(\left(k_n - k_0\right)\left((x-x_f) - c_{g,0}(t-t_f)\right)\right)}, \tag{7}$$

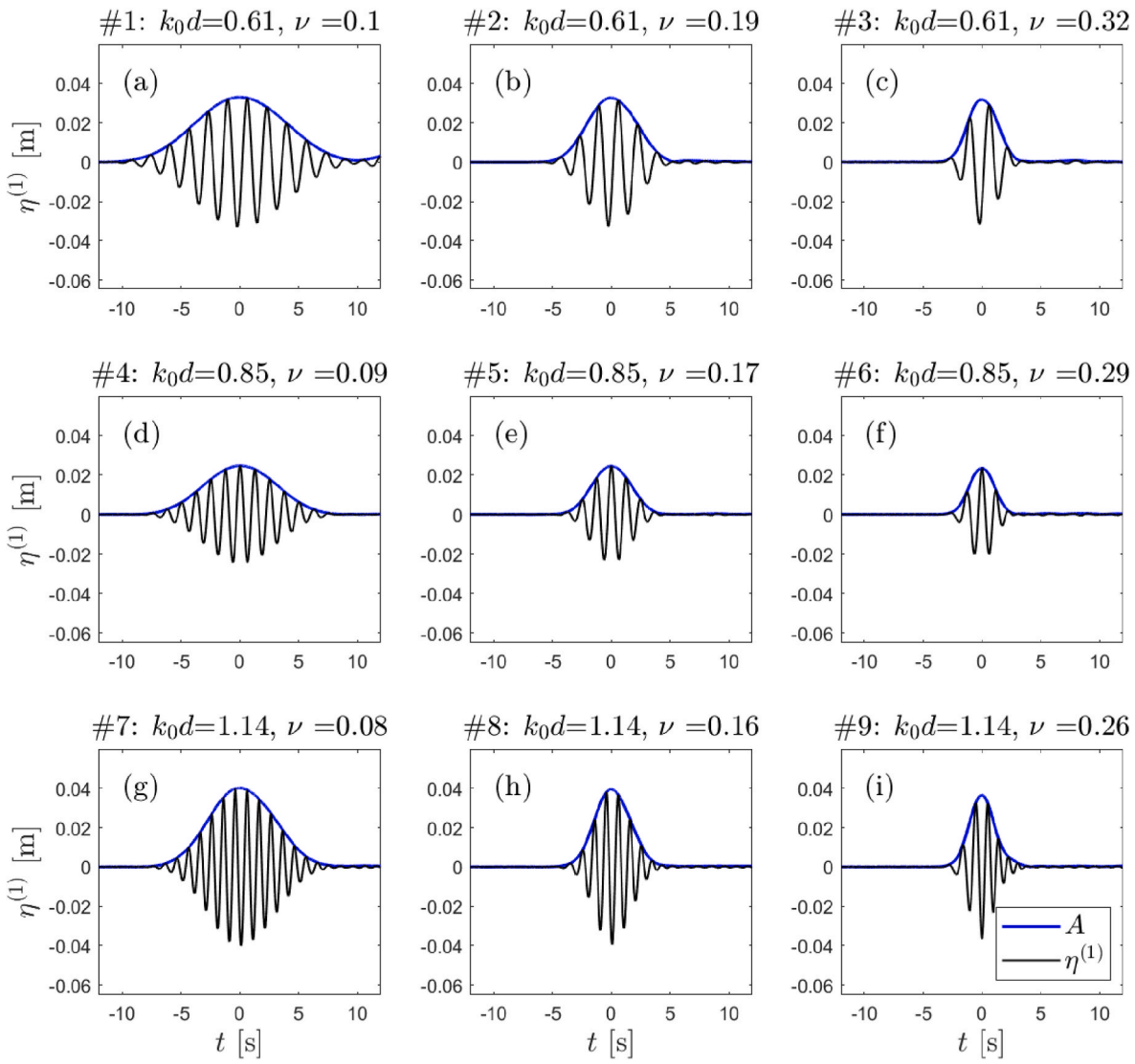

Fig. 4. Measured first-order surface elevations at wave gauge 2 (black lines) for the nine experiments with the group envelopes (blue lines) obtained using a Hilbert transform.

where ω_0 and k_0 are now the carrier wave's angular frequency and wavenumber, respectively, chosen to correspond to the spectral peak, and the (complex) envelope $A(x - c_{g,0}t)$ travels with the group velocity (without focusing, consistent with the narrow-bandwidth approximation). The group velocity is given by $c_{g,0} = nc_{p,0}$ with

$$n = \frac{1}{2} + \frac{k_0 d}{\sinh(2k_0 d)}. \tag{8}$$

The envelope (or modulation) A varies on much greater spatial and temporal scales than the carrier wave.

Mei (1989) gives the compatible (i.e., narrow-banded) second-order sub-harmonic surface elevation as

$$\eta^{(-2)} = -\frac{g|A|^2}{2(gd - c_{g,0}^2)}\left(\frac{2c_{g,0}}{c_{p,0}} - \frac{1}{2}\right), \tag{9}$$

where $c_{p,0} = \omega_0/k_0$ is the phase speed of the carrier wave. The second-order sub-harmonic (or 'wave-averaged') surface elevation eq. (9) has the appearance of a wide trough and is known as the set-down (Longuet-Higgins and Stewart, 1962). The set-down is forced by and slaved to the first-order wave group A and can therefore be described as bound, propagating at the group celerity $c_{g,0}$ with the first-order wave group A.

The occurrence of a set-down can be readily explained, using the unsteady Bernoulli equation, as the surface manifestation of the wave-induced return flow running beneath the wave group in the negative x-direction (e.g., Calvert et al. (2019)) or in terms of radiation stresses (Longuet-Higgins and Stewart, 1962). In shallower water depths, the return flow, which is driven by the divergence of the Stokes transport on the scale of the wave group, must be 'returned' or 'funneled' through a shallower depth, increasing the magnitudes of the (negative) return flow velocity and thus of the set-down.

To generate this set-down (i.e., eq. (9)), Van Leeuwen and Klopman (1996) (see also Klopman and Van Leeuwen (1990)) show that the sub-harmonic paddle displacement signal (for a piston wavemaker) is given as

$$X_{p,\text{periodic}}^{(-2)} = -\frac{gc_{g,0}}{2d(c_{g,0}^2 - gd)}\left(2n - \frac{1}{2}\right)\int_{-T/2}^{t}\left(|A(\tau)|^2 - \overline{|A|^2}\right)\mathrm{d}\tau, \tag{10}$$

where we have set $x = 0$ (cf. the wavemaker's location) in the envelope A and we have chosen a time-periodic signal $t = (-T/2, T/2)$ with repeat period T. In eq. (10), the term $\overline{|A|^2} = (1/T)\int_{-T/2}^{T/2}|A|^2\mathrm{d}\tau$ ensures the sub-harmonic paddle signal is periodic, and the paddle returns to its original position after generating the wave. For isolated wave groups, which

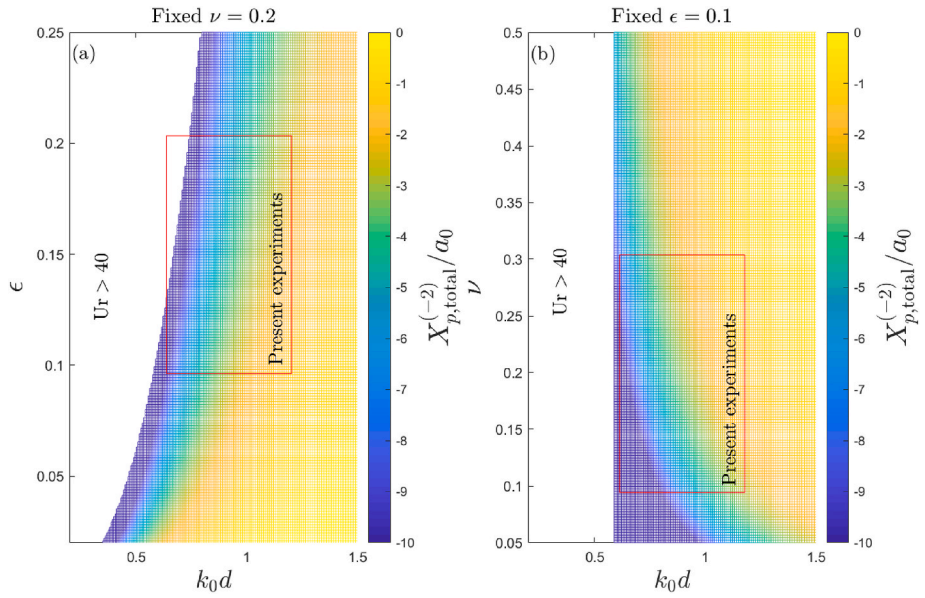

Fig. 5. Non-dimensional total backward paddle displacement: (a) as a function of relative water depth $k_0 d$ and steepness ε for fixed bandwidth ν and (b) as a function of relative water depth $k_0 d$ and bandwidth ν for fixed steepness ε. The present experimental range is indicated with red squares. The region in which the Ursell number is greater than 40 is blanked out and indicated as Ur $>$ 40.

correspond to the limit of an infinite repeat period (i.e., $T \to \infty$), this term can be ignored, and the non-periodic sub-harmonic paddle signal is given by

$$X_p^{(-2)} = -\frac{g c_{g,0}}{2d(c_{g,0}^2 - gd)} \left(2n - \frac{1}{2}\right) \int_{-\infty}^{t} |A(\tau)|^2 \mathrm{d}\tau, \tag{11}$$

We can obtain the net (backward) paddle displacement accumulated over the course of generating an isolated wave group by letting $t \to \infty$ in eq. (11).

Fig. 1 illustrates the first and second-order paddle displacement times series for a Gaussian wave group. Fig. 1a shows the first-order paddle displacement $X_p^{(1)}$ as a function of time, which shows the isolated wave group. Fig. 1b compares the periodic $X^{(-2)}_{p,\mathrm{periodic}}$ (for $T = 32$ s) and non-periodic $X_p^{(-2)}$ sub-harmonic paddle displacement. Although it is evident that the periodic and non-periodic sub-harmonic signals both display a backward motion at the same speed at the centre of the group (at $t = 0$), the periodic signal readily returns to zero on both sides of the group, giving rise to a saw-tooth-like profile. Such a periodic signal can create the set-down correctly for isolated groups (Orszaghova et al., 2014), but requires a long repeat period for the paddle's restoration to zero not to generate significant sub-harmonic motion of its own. In our experiments, we used the non-periodic sub-harmonic paddle signal, and then restored the paddle position to zero after each experiment. Finally, Fig. 1c shows the summation of first and second-order paddle displacement. Also shown in Fig. 1 are the second-order super-harmonic paddle displacements $X_p^{(+2)}$, which we include in all our experiments, but do not focus on in this paper (see Van Leeuwen and Klopman (1996) for details).

2.3. Error waves

If the correct sub-harmonic paddle displacement is not included, the physical response to the disparity in the boundary condition at second order is the formation of an error wave in the form of a sub-harmonic hump, which cancels out the set-down at the wave maker. Unlike the set-down, the error wave satisfies the linear dispersion relation, and propagates at the shallow-water wave speed ($\sqrt{gd}$). This results in the error wave being 'free' to propagate ahead of the linear wave group. In practice, the finite length of experimental flumes means that the sub-harmonic error wave typically does not have time to separate out from the linear group (e.g., Calvert et al. (2019)) and instead appears superimposed on the group set-down.

For completeness, we note that, as well as a low-frequency sub-harmonic error waves, a high-frequency super-harmonic error is formed in case of first-order generation. The super-harmonic error wave propagates slower than the linear group, and is therefore typically of much less concern in coastal engineering experiments that use wave groups.

3. Experimental methodology

3.1. Experimental set-up

The present experiments were conducted in a wave flume in the COAST (Coastal, Ocean And Sediment Transport) Laboratory, at the University of Plymouth, UK. The flume is 20 m in length, 0.6 m in width, with a constant water depth of 0.23 m. Fig. 2a shows the experimental set-up. The wavemaker (photograph in Fig. 2c) is situated at one end of the flume and a 3 m-long energy dissipating beach with a 1 : 2.5 uniform slope at the other end. Current circulation ducts at each end of the flume were completely sealed off to avoid unwanted flow. All experimental locations are referenced from the paddle resting position at $x = 0$ m. In between the wavemaker and beach, eight resistance-type wave gauges measured the free surface elevation at 128 Hz. The gauges were located along the central line of the flume, and their x-locations are denoted in the table in Fig. 2. A three-point gauge calibration, over a vertical range of 10 cm, was performed each morning prior to tests. Data acquisition from all eight wave gauges was triggered simultaneously with the wave paddle displacement time series.

3.2. Prototype wavemaker

The wavemaker (photograph in Fig. 2c) was designed and built by Edinburgh Designs Ltd (EDL) and has an x-displacement range of ± 0.8 m. It is wet-back and comprises a carriage with four independent wheels connected to two stainless steel rails mounted on the sides of the flume. The carriage is driven by an electrical motor with a rack and pinion system. The paddle is operated through displacement control according to a pre-defined paddle displacement time series. This allows for

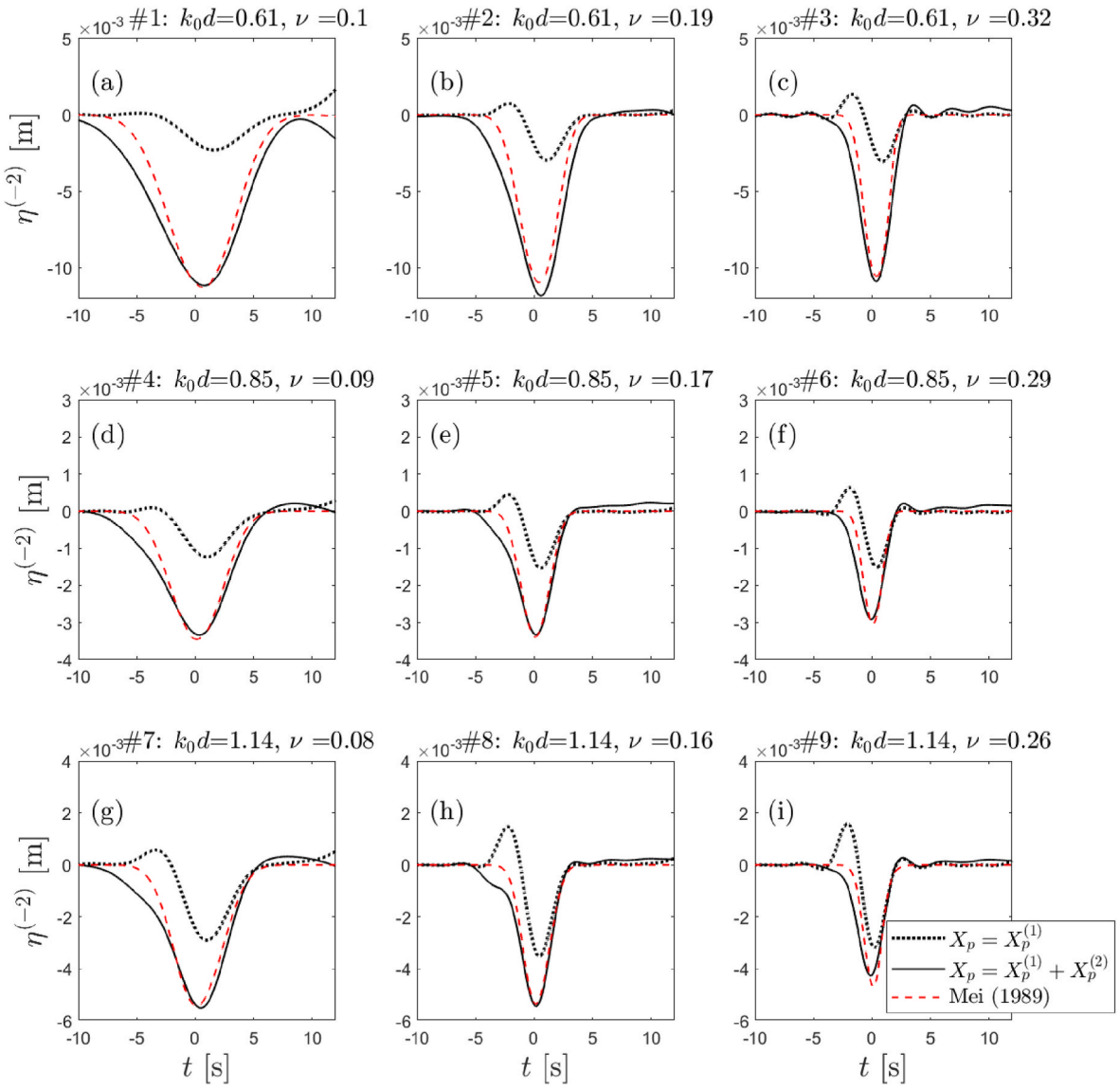

Fig. 6. Sub-harmonic surface elevation at wave gauge 2 for the nine experiments showing results for first-order generation (dotted black lines), second-order generation (solid black lines), and the theoretically predicted set-down of Mei (1989) (dashed red lines) computed using eq. (9).

generation of non-periodic paddle signals, such as used in our experiments for isolated wave groups.

Fig. 2b shows the impermeable seal placed around the edges and base of the paddle face. The seal was designed to retain a head of water across the paddle face for an extended period of time. A key finding from preliminary calibration experiments is that to generate the sub-harmonic surface elevation correctly, it is critical to maintain the volume of water behind the paddle, preventing water leaking forwards around the paddle face, which can result in additional sub-harmonic error waves at late times. The final seal design comprised a dual layer of semi-rigid plastic film with petroleum grease lubricating the boundary with the flume wall. After each experiment, the paddle position was restored to $x = 0$ m. A 10 min settling period was held between each experiment to let residual energy dissipate. A small foam dissipative beach installed behind the paddle face reduced seiche effects in the wet-back area.

3.3. Experimental matrix

Table 2 shows the experimental matrix of the nine wave group experiments we have conducted. Each experimental case was generated twice, once using purely first-order paddle displacement and again with the additional second-order correction applied, where we use a non-periodic sub-harmonic signal eq. (11). We chose signals with Gaussian wave groups of the form

$$A = a_0 \exp\left(-\frac{\left((x - x_f) - c_{g,0}(t - t_f)\right)^2}{2\sigma^2} \right), \tag{12}$$

where σ is the characteristic length scale of the wave group. Three non-dimensional numbers characterise each experiment: the non-dimensional water depth $k_0 d$, the steepness $\varepsilon = k_0 a_0$ and the bandwidth $\nu = \sqrt{m_2 m_0 / m_1^2 - 1}$, where m_n is the nth moment of the energy spectrum. For Gaussian groups, the energy spectrum $S(\omega)$ of the surface elevation can be readily evaluated in closed form:

$$S(\omega) = \frac{\sigma^2 a_0^2}{4\sqrt{\pi} c_{g,0}} \exp\left(-\frac{(\omega - \omega_0)^2 \sigma^2}{4 c_{g,0}^2} \right), \tag{13}$$

from which the bandwidth parameter ν can be obtained: $\nu = \sqrt{2} c_{g,0} / (\sigma \omega_0) = \sqrt{2} n / (k_0 \sigma)$.

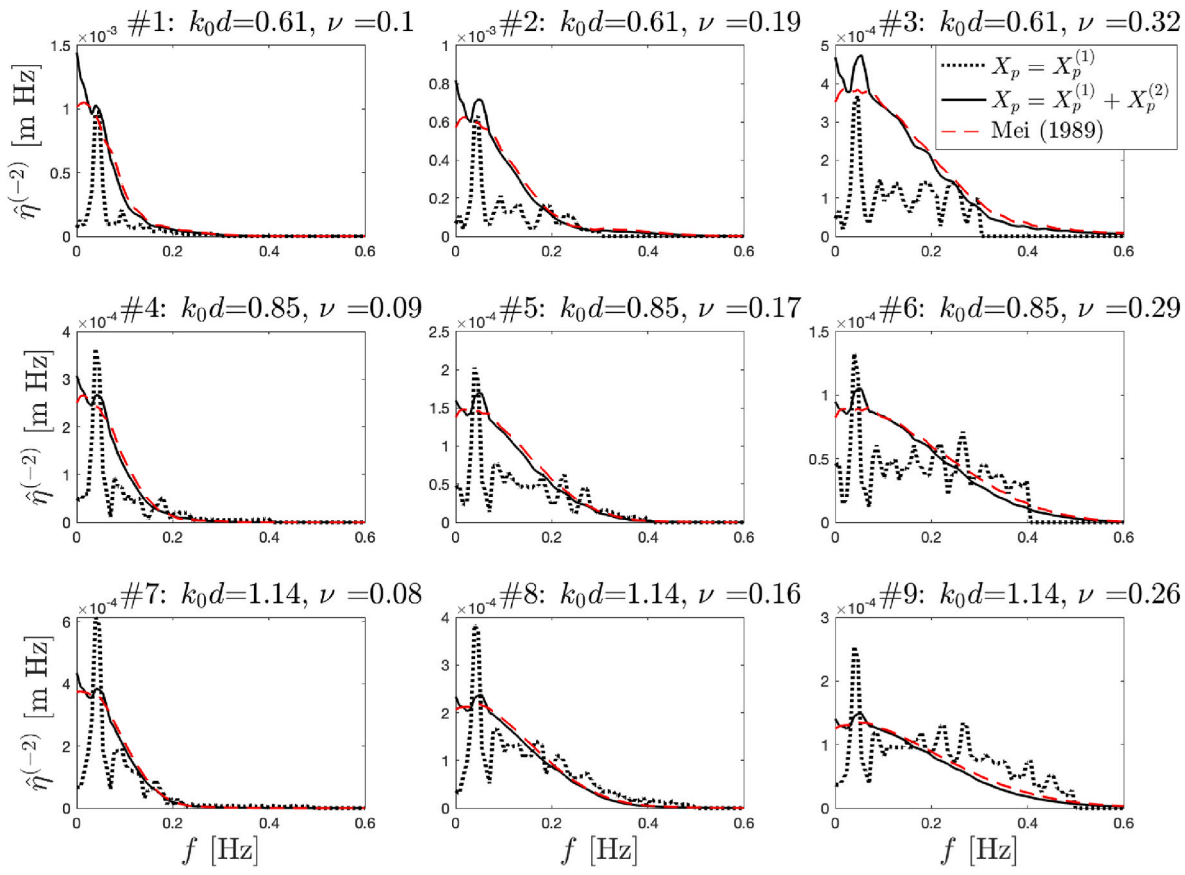

Fig. 7. Frequency spectra for the sub-harmonic contribution to all nine experiments showing results for first-order generation (dotted black lines), second-order generation (solid black lines), and the theoretically predicted set-down of Mei (1989) (dashed red lines) computed using eq. (9).

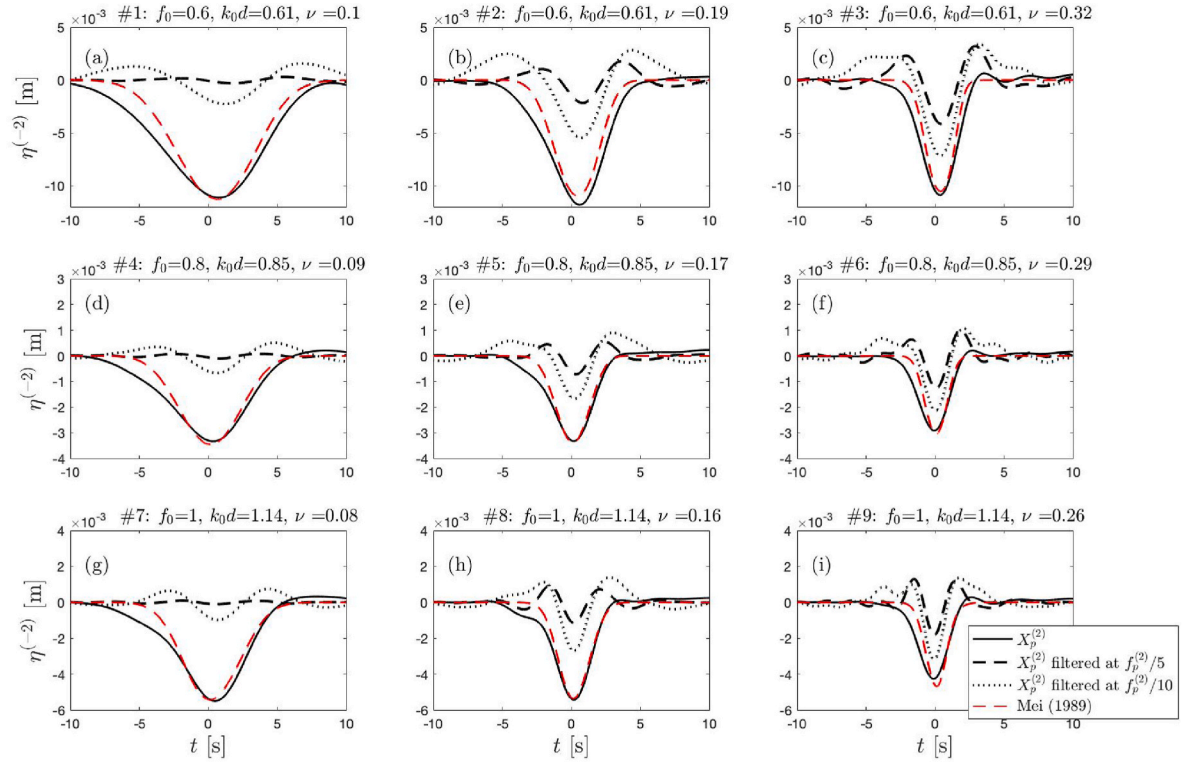

Fig. 8. The sub-harmonic measured surface elevation with second-order generation after filtering with the same high-pass limits as in Janssen et al. (2003).

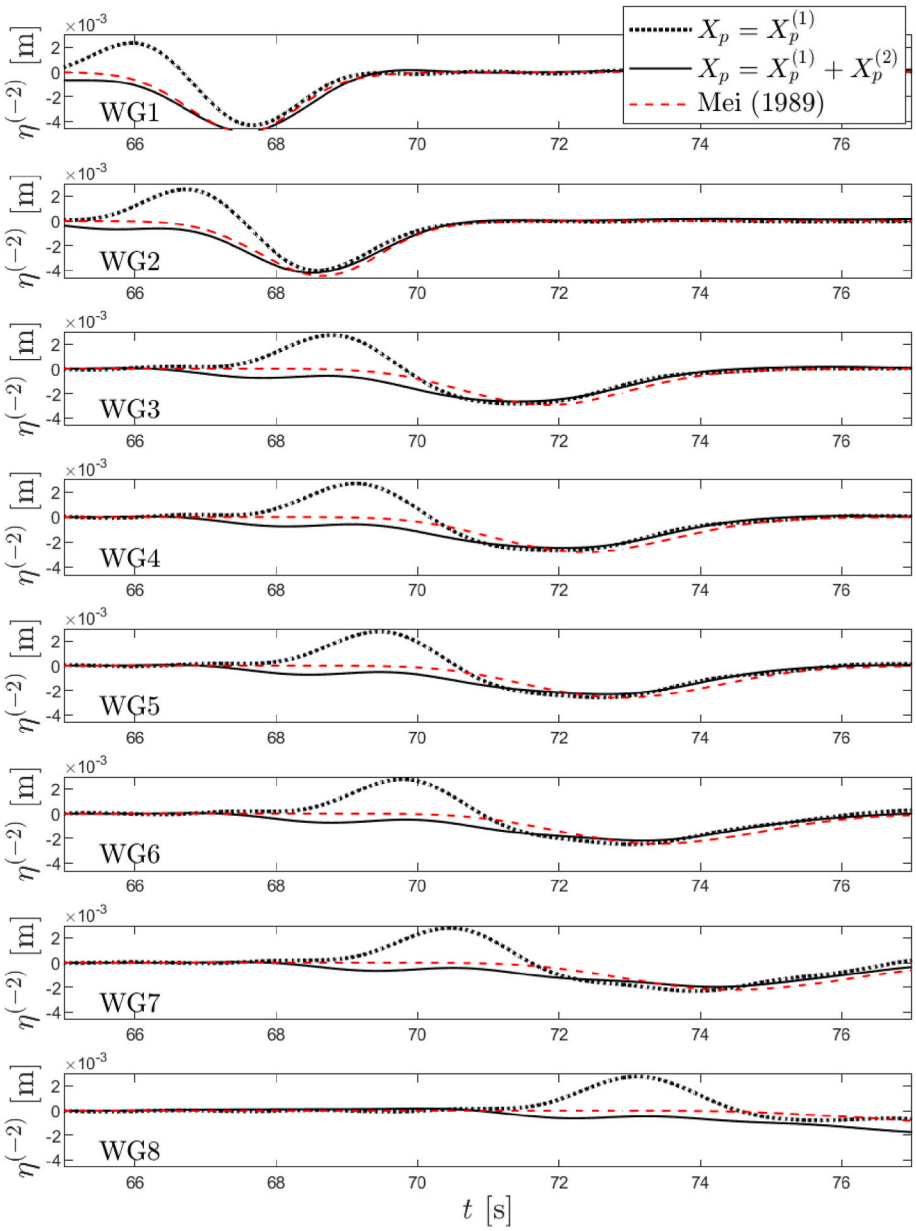

Fig. 9. Sub-harmonic surface elevation for experiment 9 at all 8 wave gauges (WG) showing the two different generation methods: first-order generation (dotted black lines) and second-order generation (solid black lines). Also shown is the theoretically predicted set-down of Mei (1989) (dashed red lines) computed using eq. (9).

Our experimental matrix consisted of three peak frequencies (f_0 = 0.6, 0.8, 1.0 Hz), corresponding to shallow to intermediate relative water depths ($k_0 d$ = 0.6, 0.9, 1.1). For each frequency, we considered three bandwidths. The bandwidths were chosen so that the groups remained quasi-monochromatic, but sufficiently compact in time and space for any sub-harmonic error waves to separate out from the first-order group. Each experimental run had a duration of T = 128 s, x_f = 4.5 m, and $t_f = T/2$.

3.4. Separation of harmonics

To separate the second-order sub-harmonic waves from the first-order waves, we use the so-called two-phase harmonic extraction (or phase inversion) technique (Baldock et al. (1996), see also Hunt (2003)). To do so, we carry out each experiment in duplicate form, with a group focusing to a crest ($\eta_0(t)$) and a group focusing to a trough ($\eta_{180}(t)$). Specific combinations of the two inverted group time-series can yield the odd and even powers in amplitude, such that:

$$\eta_{\text{odd}} = \frac{\eta_0 - \eta_{180}}{2} \quad \text{and} \quad \eta_{\text{even}} = \frac{\eta_0 + \eta_{180}}{2}. \tag{14}$$

To leading order, η_{odd} is dominated by the first-order (in steepness) signal, and η_{even} by the second-order (in steepness) signal in an underlying Stokes expansion. The latter is made up from bound waves and free error waves at second-order.

Fig. 3 illustrates the separation of harmonics method. Each harmonic contribution is displayed in both the time and the frequency domain. The top left (Fig. 3a) shows a crest-focused (η_0) and trough-focused (η_{180}) wave group measured within the flume. The top right (Fig. 3b) shows the decomposition of the amplitude spectrum into odd (η_{odd}) and even (η_{even}) components. The subsequent panels (Fig. 3c–j) separately display the different components, which have been isolated using a band-pass filter. The components are divided up into: second-order sub-harmonic components ($\eta^{(-2)}$) obtained from band-pass filtering η_{even}

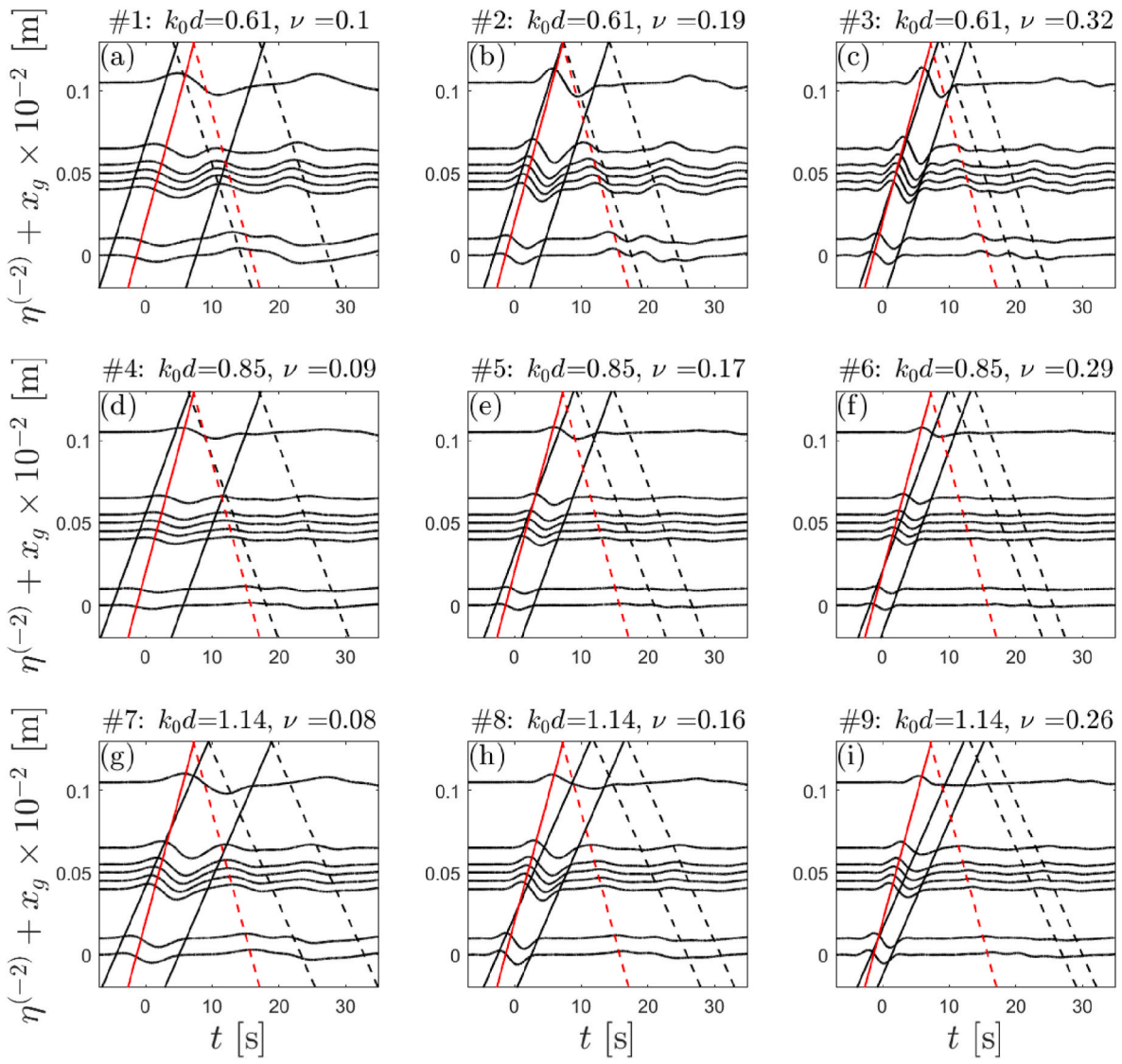

Fig. 10. For first-order accurate generation, spatio-temporal evolution of the sub-harmonic surface elevation at each wave gauge, vertically offset by the gauge location (x_g). The continuous red lines indicate sub-harmonic error wave speed ($c_e = \sqrt{gd}$), the black lines indicate the group width (2σ), travelling at the group speed ($c_{g,0}$); the dashed lines indicate their respective reflections.

between 0 and 0.5 Hz; first-order components ($\eta^{(1)}$) obtained from band-pass filtering η_{odd} between $0.5f_0 - 1.5f_0$; second-order super-harmonic components ($\eta^{(+2)}$) obtained from band-pass filtering η_{even} between $1.5f_0 - 2.5f_0$; and third- (or higher) order components ($\eta^{(3)}$) obtained from band-pass filtering η_{odd} between $2.5f_0 - 3.5f_0$. For the sub-harmonic time series thus obtained, the error wave crest is labelled, preceding ahead of the set-down trough in Fig. 3c for this first-order generated group. Fig. 3i–j illustrate the negligible contribution at third order.

3.5. First-order wave groups

Fig. 4 shows the linearised wave groups at wave gauge 2 for all nine experimental cases with the envelopes obtained using a Hilbert transform also shown. Moving from left to right, the groups have increasing bandwidth, evident in the time domain as a group that is made up from fewer waves. The first-order surface elevations measured are equivalent for both the first and second-order generation methods.

3.6. Maximum paddle displacement

As shown in Equation (11), we obtain the net (backward) paddle displacement over the course of generating an isolated wave group by letting $t \to \infty$ (i.e., $\Delta X_{p,\text{total}}^{(-2)} = X_p^{(-2)}(t \to \infty)$):

$$\frac{\Delta X_{p,\text{total}}^{(-2)}}{a_0} = -\sqrt{\frac{\pi}{2}}\frac{\varepsilon n}{\nu}\frac{2n-1}{(k_0d)^2\left(\frac{\tanh^2(kh)}{kh}n^2-1\right)}, \tag{15}$$

where we have used the properties of a Gaussian group to evaluate the integral in eq. (11) in closed form. Equation (15) gives the non-dimensional total backward paddle displacement $\Delta X_{p,\text{total}}^{(-2)}/a_0$ as a function of three non-dimensional groups (nb. $n = n(k_0d)$ through eq. (8)): the relative depth k_0d, the steepness ε, and the bandwidth parameter ν.

Table 2 gives the total backward paddle displacement for the different experiments, demonstrating the paddle displacement is greatest for the shallowest (smallest k_0d) and most narrow-banded (smallest ν) experiments. Fig. 5 shows the non-dimensional total backward paddle displacement $X_{p,\text{total}}^{(-2)}/a_0$ as a function of relative water depth k_0d and

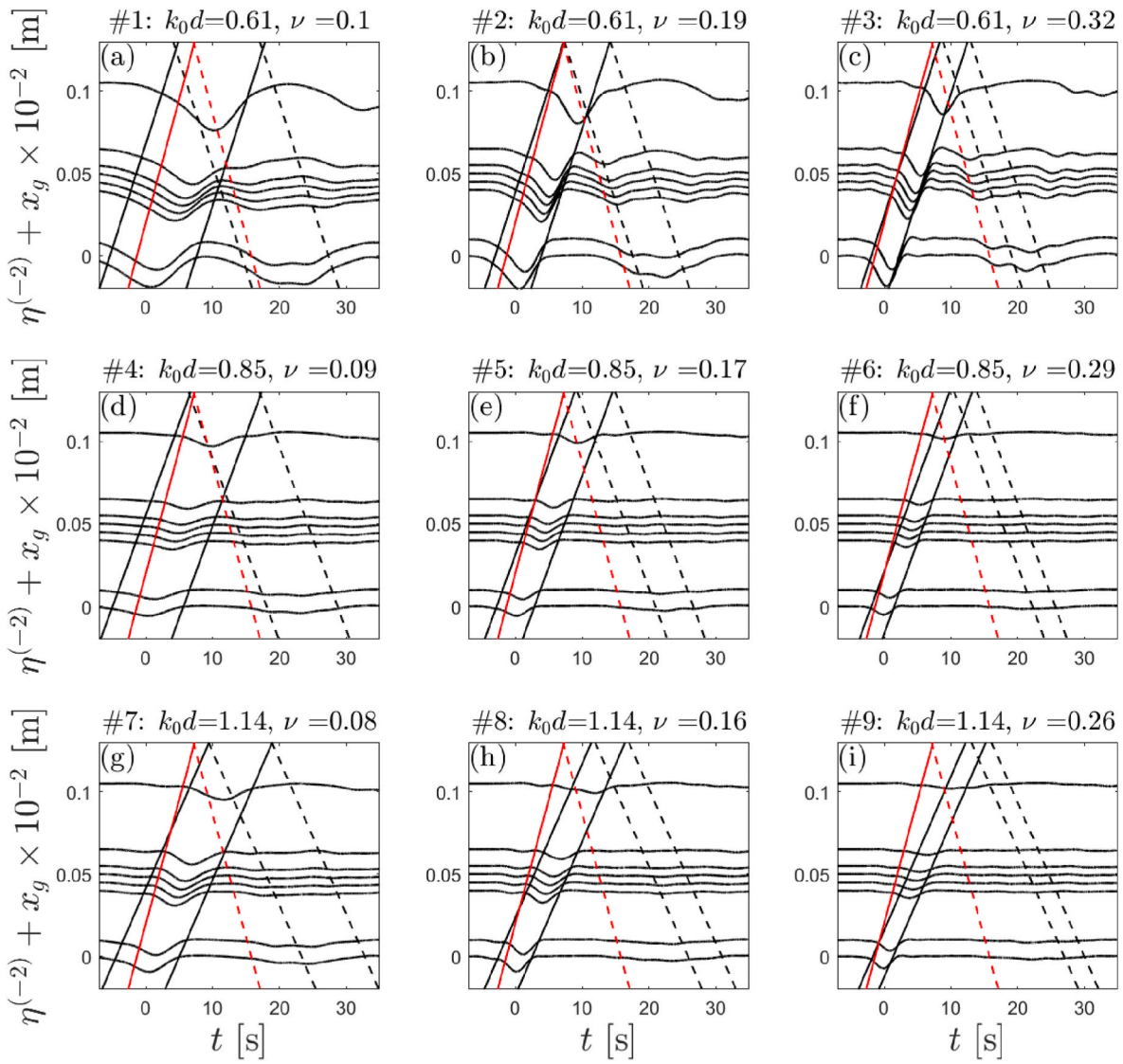

Fig. 11. For second-order accurate generation, spatio-temporal evolution of the sub-harmonic surface elevation at each wave gauge, vertically offset by the gauge location (x_g). The continuous red lines indicate sub-harmonic error wave speed ($c_e = \sqrt{gd}$), the black lines indicate the group width, travelling at the group speed ($c_{g,0}$); the dashed lines indicate their respective reflections.

steepness ε for fixed bandwidth ν (Fig. 5a) as a function of relative water depth k_0d and bandwidth ν for fixed steepness ε (see, Fig. 5b). It is evident from Fig. 5 that the total net backward paddle displacement can be significantly larger than the linear wave amplitude, up to seventeen times observed in experiment 1, and increases rapidly as the relative water depth becomes shallower or the bandwidth decreases.

Within both panels of Fig. 5, values of the total backward displacement are not shown for Ursell numbers greater than 40, with the Ursell number defined as

$$\mathrm{Ur} = \frac{H\lambda_0^2}{d^3} = \frac{8\pi^2\varepsilon}{(k_0d)^3}, \tag{16}$$

where $\lambda_0 = 2\pi/k_0$. The Ursell number indicates the relative importance of nonlinearity in shallow water depths. Ur $>$ 40 typically indicates regions where nonlinearity beyond second order becomes important and cnoidal wave theories need to be considered, which is beyond the scope of the present paper.

4. Results

4.1. Bound second-order set-down

Fig. 6 shows the measured sub-harmonic surface elevations for both first-order and second-order accurate wave generation compared to the theoretically predicted set-down according to Mei (1989) given in eq. (9). It is worth noting that the theoretical set-down given by Mei's expression is congruent with the set-down given by the full second-order (broad-banded) theory for all our experimental cases (shown in fig. B14, included as an appendix). The measurements in Fig. 6 are recorded at wave gauge 2 (x = 4.5 m). The second-order generated sub-harmonics appear to match the theoretical set-down by Mei (1989) very well, especially at the centre of the group. The second-order generated cases do not show the preceding free error wave, which is clearly present as a set-up for the first-order generated cases. The first-order generated sub-harmonics shows poor agreement with the theoretical set-down. The free error wave is shown to be contaminating the first-order set-down in all nine cases, appearing as a set-up between $t = -4.0$ and -2.0 s. After the group has passed, the second-order generated sub-harmonic surface elevation returns to the original still water level. The slight

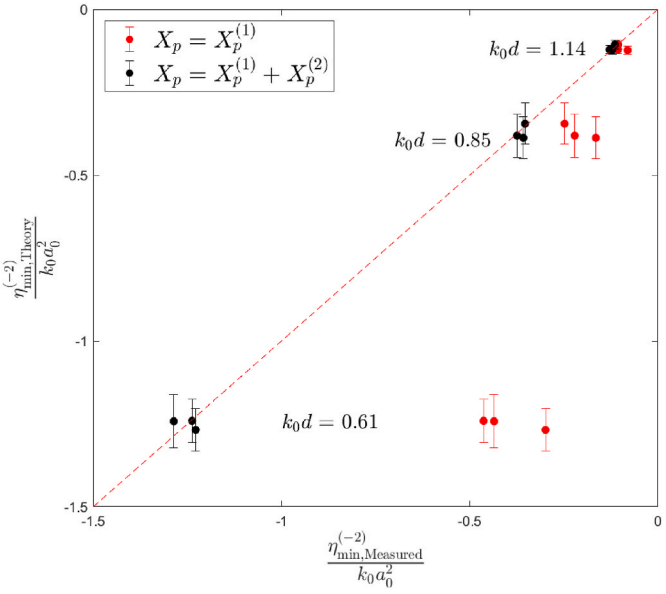

Fig. 12. Measured set-down amplitude $\eta^{(-2)}_{\text{min,Measured}}$ against the theoretical prediction $\eta^{(-2)}_{\text{min,Theory}}$ for all nine first-order and second-order generated cases. Error bars indicate ±2 standard deviation around the mean, obtained from five repeats.

increase in the water level after the group has passed is likely caused by a slow leaking forwards of the water held behind the wave paddle.

Fig. 7 shows the sub-harmonic frequency contributions of the same nine experimental cases as displayed in Fig. 6. Again, the figure compares first-order generated, second-order generated, and theoretically derived subharmonic for of the nine wave group cases. The figure shows that, just as in time (e.g., Fig. 6) there is good agreement in frequency space between the second-order generated groups and the theoretical prediction given by Mei (1989). Whereas, the first-order generated groups are seen to have poor agreement with theory.

Fig. 8 shows how limited stroke length can lead to unacceptable errors. We have demonstrated this by applying the same limits ($f_p/5$ and $f_p/10$, where f_p is the peak frequency) in a high-pass filter to the measured sub-harmonic surface elevation $\eta^{(-2)}$ as Janssen et al. (2003), who applied these limits in view of restrictions imposed by the limited excursion of the wave board in their experiments. The figure shows that applying a frequency filter based on those frequencies identified by Janssen et al. (2003) as potentially affected by paddle stroke limitations leads to a significant departure between the measured and the theoretically predicted set-down for our experiments. This departure is of course greater for $f_p/5$ than for $f_p/10$. The effect also clearly depends on the band-width of the group. Broad-banded groups (Fig. 8c,f,i) are affected much less than narrow-banded groups (Fig. 8a,d,g), which is explained by the fact that sub-harmonic bound waves for broad-banded waves are spread over a much broader range of frequencies and comparatively less energy is consequently removed by a high-pass filter. In the spatial domain, the correct sub-harmonic for narrow-banded groups simply requires a much greater stroke length (see Fig. 5).

Fig. 9 shows results from experiment 9 (the case with the narrowest characteristic group width σ and the slowest linear group speed $c_{g,0}$) at wave gauge 2, and gives the best view of incident wave sub-harmonics prior to contamination by reflections. In the first-order generated sub-harmonic time series, we see the superposition of the error wave upon the set-down, and disagreement with the theoretical result of Mei (1989). Fig. 9 shows the error wave separating out ahead of the set-down at progressive wave gauge locations; eventually, the set-down magnitudes of both first-order and second-order generation begin to match the theory once the error wave has separated out ahead, but before reflections become dominant.

Fig. 10 and Fig. 11 respectively show the spatio-temporal evolution of the sub-harmonic surface elevation for the first-order and the second-order generated cases. It is evident from both figures that the bound set-down propagates with the same celerity as the linearised wave group $c_{g,0}$ (continuous black line at a distance of 2σ apart corresponding to characteristic group width). Fig. 10 shows the free error wave satisfies the dispersion relation and propagates with the speed of a shallow-water wave $c_e = \sqrt{gd}$ (continuous red line). These two speeds (i.e., $c_{g,0}$ and $c_e = \sqrt{gd}$) are similar in magnitude for the shallower cases, so that the error wave no longer separates out. The reflections of the error wave and set-down are indicated by dashed lines in their respective colours. The absence of error waves and their reflections in Fig. 11 confirms second-order accurate generation has been successful in all nine experiments.

Fig. 12 compares the measured set-down amplitude $\eta^{(-2)}_{\text{min,Measured}}$ of both first-order (red dots) and second-order (black dots) generated wave groups with theoretically predicted second-order correct amplitude $\eta^{(-2)}_{\text{min,Theory}}$, all normalized by $k_0 a_0^2$. The relative water depths of our experiments are indicated on the plot as well as a one to one agreement between measurements and theory (red dashed line). Error bars mark ±2 standard deviations around the mean obtained from 5 repeats. Fig. 12 shows that in our deepest cases ($k_0 d = 1.14$) we see only a slight difference between the set-down amplitude produced by first and second-order generation, and generally good agreement with theory. Yet, in shallower cases ($k_0 d = 0.6$–0.85) we see an increasing difference between first- and second-order generated cases. Measured second-order generated cases shows excellent agreement with theory at all depths, whereas the measured first-order generated cases are increasingly in disagreement with theory at shallower depths.

Appendix A displays the repeatability of five repeats of experiments #1–6. The red-dashed line again shows the theoretical set-down given by Mei (1989) with the mean of the five repeats and two standard deviations around the mean. The repeatability is shown to be excellent in all cases.

5. Conclusion

Second-order wave generation theory has been established for nearly three decades, and numerous studies have partially or fully implemented the theory for bichromatic and irregular wave experiments. Different from previous studies, we validate second-order wave theory explicitly for isolated wave groups in shallow to intermediate water depth ($k_0 d = 0.6$–1.1). Previously this has only been achieved in deeper water with Sriram et al. (2015) only examining wave groups in intermediate to deep water ($k_0 d = 1.5$–3.4) and Whittaker et al. (2017) only achieving a 60% reduction of the sub-harmonic free error wave amplitude in shallow water ($k_0 d = 0.7$).

As water depth is reduced, stroke-length of the wavemaker becomes an important limiter in applying second-order wave theory, as noted by Whittaker et al. (2017). This is due to the required backward displacement of the wavemaker to correctly reproduce the set-down. We show that this backward displacement can readily exceed seventeen times the amplitude of the first-order group in shallow cases. In the present work, we have implemented a prototype wavemaker with an extended paddle stroke to enable us to reproduce the correct set-down for isolated groups in shallow water depths. To do so, we have applied the narrow-banded second-order wavemaker theory of Van Leeuwen and Klopman (1996), which has proven to be simple and efficient to compute in closed form, making its implementation to a laboratory wavemaker highly suitable to a broad range of users for different coastal engineering applications. Particularly, studies using isolated wavepackets as a design conditions for extreme wave-structure interactions.

Through analysis of the harmonic structure of a range of wave groups, varying in peak frequency and spectral bandwidth, we have

shown that the measured sub-harmonics are in excellent agreement with the theoretically predicted sub-harmonic free surface elevation (e.g., Mei (1989)). As further evidence of this agreement, the sub-harmonic error wave that normally travels ahead of the first-order group and contaminates experimental wave fields using first-order generation (e.g., Orszaghova et al. (2014)) are entirely eliminated. During our application of second-order correct paddle displacement, we have found it to be essential to have a seal around the paddle face, to maintain a water head during the paddle's movement and prevent leakage of water around the paddle face.

Future work will use the newly implemented paddle and theory to quantify the implications of second-order correct focused wave groups, free of second-order error waves, for wave-structure interaction studies, in particular, run-up and wave loading on vertical structures.

CRediT authorship contribution statement

William Mortimer: Experiment set-up, Data collection, Writing – original draft, Formal analysis. **Alison Raby:** Formal analysis, Supervision. **Alessandro Antonini:** Formal analysis, Supervision. **Deborah Greaves:** Formal analysis, Supervision. **Ton S. van den Bremer:** Formal analysis, Supervision.

Declaration of competing interest

The authors declare that they have no known competing financial interests or personal relationships that could have appeared to influence the work reported in this paper.

Acknowledgements

The authors acknowledge support from Edinburgh Designs Ltd, who have contributed their prototype piston-type wavemaker at zero cost as part of the ongoing collaborative development of their new wavemaker. We would like to thank the COAST laboratory technicians for their help in installing the wavemaker. WM received PhD funding from the COAST laboratory at the University of Plymouth. TSvdB was supported by a Royal Academy of Engineering Research Fellowship. The authors are grateful to M.L. McAllister and R. Calvert for their assistance implementing second-order theory and P.H. Taylor and A.G.L. Borthwick for discussions that led to the piston-type wavemaker development.

Appendix A. Repeatability

To assess repeatability and obtain an estimate of experimental error, fig. A13 shows the mean sub-harmonic free-surface elevation taken from five repeats of second-order generated wave groups, measured at wave gauge 2 (black lines), a confidence band of ±2 standard deviations around the mean (blue lines) and the theoretically predicted set-down according to Mei (1989) (red lines) for experiment 1–6. The six experimental cases show excellent repeatability, even when the sub-harmonic amplitude is < 3 mm. The confidence bands of all six experimental cases capture the magnitude of theoretical set-down maximum well with minor differences in shape in the time-domain between the measured and predicted set-down.

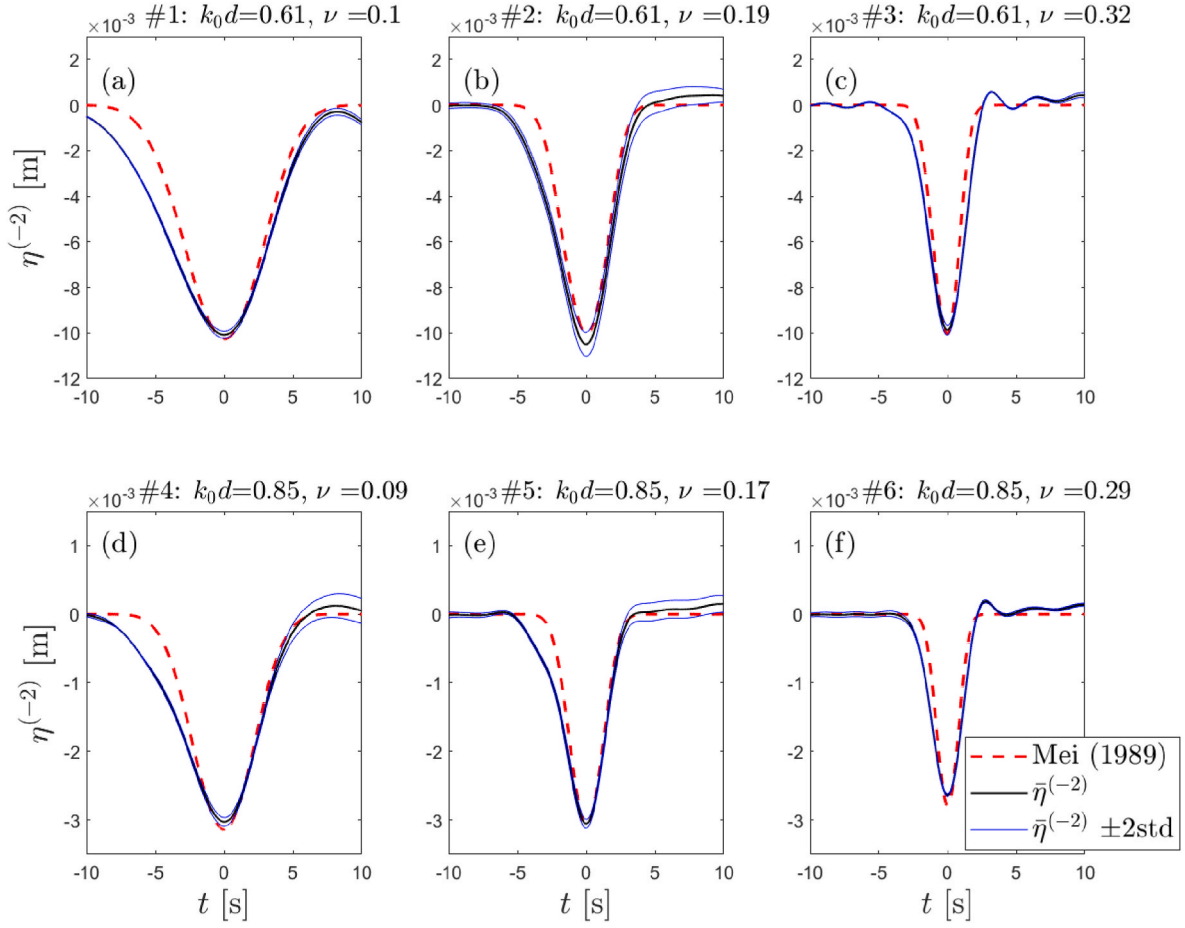

Fig. A.13. Sub-harmonic second-order generation repeatability in experiments 1–6. The mean of five repeats (black line), 2 standard deviations (±2std) around the mean (blue lines), the theoretical set-down according to Mei (1989) (red dashed line).

Appendix B. Narrow and broad-banded set-down comparison

Figure B14 is similar to the previously seen Fig. 6, but includes the broad-banded second-order free surface, which is given as the wave-averaged free-surface of a broad banded group in eq. (2.4) in McAllister et al. (2018). Figure B14, shows that there is a high degree of congruence between the broad-banded and narrow-banded second-order subharmonic.

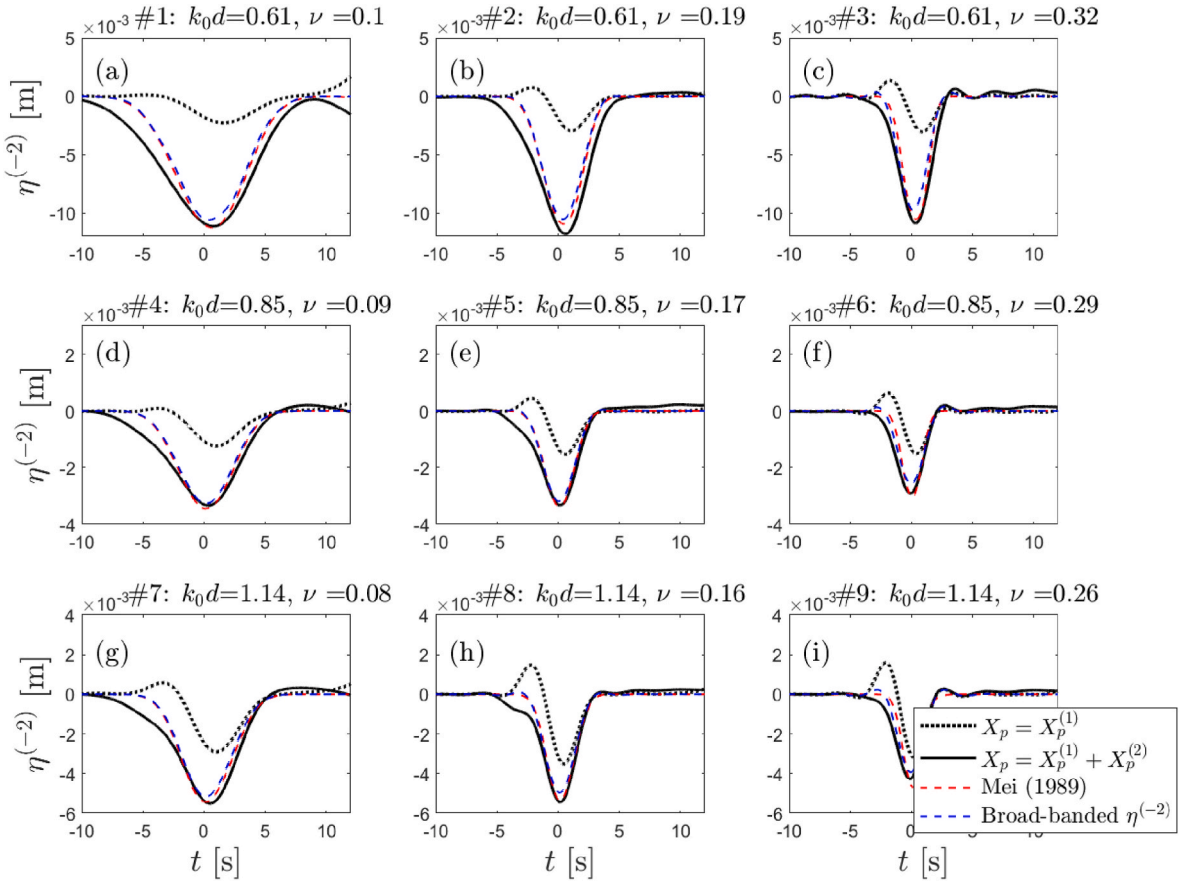

Fig. B.14. Similar to Fig. 6 but with the broad-banded second-order sub-harmonic surface elevation also included (blue dashed lines).

References

Abroug, I., Abcha, N., Dutykh, D., Jarno, A., Marin, F., 2020. Experimental and numerical study of the propagation of focused wave groups in the nearshore zone. Phys. Lett. 384, 126144.

Aknin, D., Spinneken, J., 2017. A laboratory investigation concerning the superharmonic free wave suppression in shallow and intermediate water conditions. Coast Eng. 120, 112–132.

Antonini, A., Archetti, R., Lamberti, A., 2017. Wave simulation for the design of an innovative quay wall: the case of Vlorë Harbour. Nat. Hazards Earth Syst. Sci. 127–142.

Baldock, T., Swan, C., Taylor, P., 1996. A laboratory study of nonlinear surface waves on water. Philos. Trans. R. Soc. London, Ser. A: Math. Phys. Eng. Sci. 354, 649–676.

Baldock, T., Huntley, D., Bird, P., O'hare, T., Bullock, G., 2000. Breakpoint generated surf beat induced by bichromatic wave groups. Coast Eng. 39, 213–242.

Barthel, V., Mansard, E.P., Sand, S.E., Vis, F.C., 1983. Group bounded long waves in physical models. Ocean Eng. 10, 261–294.

Battjes, J., Bakkenes, H., Janssen, T., van Dongeren, A., 2004. Shoaling of subharmonic gravity waves. J. Geophys. Res.: Oceans 109.

Biésel, F., Suquet, F., 1951. Les appareils générateurs de houle en laboratoire. La houille blanche 147–165.

Boccotti, P., 1983. Some new results on statistical properties of wind waves. Appl. Ocean Res. 5, 134–140.

Boccotti, P., 1989. On mechanics of irregular gravity waves. Atti Accademia Nazionale dei Lincei, Memorie viii 111–170.

Boccotti, P., 2000. Wave Mechanics for Ocean Engineering. Elsevier.

Boers, M., 1996. Simulation of a Surf Zone with a Barred Beach. Faculty of Civil Engineering, Delft University of Technology.

Borthwick, A.G.L., Hunt, A.C., Feng, T., Taylor, P.H., Stansby, P.K., 2006. Flow kinematics of focused wave groups on a plane beach in the UK. Coastal Research Facility 53, 1033–1044. https://doi.org/10.1016/j.coastaleng.2006.06.007.

Buldakov, E., Stagonas, D., Simons, R., 2017. Extreme wave groups in a wave flume: controlled generation and breaking onset. Coast Eng. 128, 75–83.

Calvert, R., Whittaker, C., Raby, A., Taylor, P., Borthwick, A., Van Den Bremer, T., 2019. Laboratory study of the wave-induced mean flow and set-down in unidirectional surface gravity wave packets on finite water depth. Phys. Rev.Fluids 4, 114801.

Cattrell, A., Srokosz, M., Moat, B., Marsh, R., 2019. Seasonal intensification and trends of rogue wave events on the US western seaboard. Sci. Rep. 9, 1–8.

Chan, E., Melville, W., 1988. Deep-water plunging wave pressures on a vertical plane wall. Proc. Roy. Soc. Lond.A.Math. Phys. Sci. 417, 95–131.

Chen, L., Zang, J., Taylor, P.H., Sun, L., Morgan, G., Grice, J., Orszaghova, J., Ruiz, M.T., 2018. An experimental decomposition of nonlinear forces on a surface-piercing column: Stokes-type expansions of the force harmonics. J. Fluid Mech. 848, 42–77.

Dawson, D., Shaw, J., Gehrels, W.R., 2016. Sea-level rise impacts on transport infrastructure: the notorious case of the coastal railway line at Dawlish, England. J. Transport Geogr. 51, 97–109.

Dean, G., Dalrymple, R., 1991. Water Wave Mechanics for Engineers and Scientists. Advanced Series in Ocean Eng., vol. 2. World Scientific Publishing.

Det Norske Veritas, 2010. Recommended Practice DNV-RP-C205: Environmental Conditions and Environmental Loads. DNV, Norway.

Drazen, D.A., Melville, W.K., Lenain, L., 2008. Inertial scaling of dissipation in unsteady breaking waves. J. Fluid Mech. 611, 307.

Fang, Q., Liu, J., Guo, A., Li, H., 2020. Methodology and experimental validation for generating periodic focused waves in a wave flume. Ocean Eng. 210, 107394.

Fernández, H., Sriram, V., Schimmels, S., Oumeraci, H., 2014. Extreme wave generation using self correcting method—Revisited. Coast Eng. 93, 15–31.

Flick, R.E., Guza, R.T., 1980. Paddle generated waves in laboratory channels. J. Waterw. Port, Coast. Ocean Div. 106, 79–97.

Hofland, B., Wenneker, I., Van Steeg, P., 2014. Short test durations for wave overtopping experiments. In: Proceedings of the 5th International Conference on the Application of Physical Modelling to Port and Coastal Protection, pp. 349–358.

Hunt, A., 2003. Extreme Waves, Overtopping and Flooding at Sea Defences. Ph.D. thesis. University of, Oxford.

Hunt-Raby, A.C., Borthwick, A.G., Stansby, P.K., Taylor, P.H., 2011. Experimental measurement of focused wave group and solitary wave overtopping. J. Hydraul. Res. 49, 450–464.
ISO:19901-1:2015, . Petroleum and natural gas industries - Specific requirements for offshore structures - Part 1: Metocean design and operating considerations. Technical Report. ISOInternational Organization for Standardization. Geneva, CH.
Janssen, T., Battjes, J., Van Dongeren, A., 2003. Long waves induced by short-wave groups over a sloping bottom. J. Geophys. Res.: Oceans 108.
Jonathan, P., Taylor, P.H., 1997. On irregular, nonlinear waves in a spread sea. J. Offshore Mech. Arctic Eng. 119, 37–41.
Judge, F.M., Hunt-Raby, A.C., Orszaghova, J., Taylor, P.H., Borthwick, A.G., 2019. Multi-directional focused wave group interactions with a plane beach. Coast Eng. 152, 103531.
Karmpadakis, I., Swan, C., 2020. On the average shape of the largest waves in finite water depths. J. Phys. Oceanogr. 50, 1023–1043.
Klopman, G., Van Leeuwen, P.J., 1990. An Efficient Method for the Reproduction of Non-linear Random Waves, pp. 478–488.
Lindgren, G., 1970. Some properties of a normal process near a local maximum. Ann. Math. Stat. 41, 1870–1883.
Longuet-Higgins, M., 1974. Breaking waves in deep or shallow water. In: Proc. 10th Conf. On Naval Hydrodynamics. MIT.
Longuet-Higgins, M.S., Stewart, R., 1962. Radiation stress and mass transport in gravity waves, with application to 'surf beats. J. Fluid Mech. 13, 481–504.
Martins, K., Bonneton, P., Michallet, H., 2021. Dispersive characteristics of non-linear waves propagating and breaking over a mildly sloping laboratory beach. Coast Eng. 167, 103917.
McAllister, M., Adcock, T., Taylor, P., Van Den Bremer, T., 2018. The set-down and set-up of directionally spread and crossing surface gravity wave groups. J. Fluid Mech. 835, 131–169.
Mei, C.C., 1989. The Applied Dynamics of Ocean Surface Waves, 1. World scientific.
Orszaghova, J., Taylor, P.H., Borthwick, A.G., Raby, A.C., 2014. Importance of second-order wave generation for focused wave group run-up and overtopping. Coast Eng. 94 (63), 79.
Pierella, F., Bredmose, H., Dixen, M., 2021. Generation of highly nonlinear irregular waves in a wave flume experiment: spurious harmonics and their effect on the wave spectrum. Coast Eng. 164, 103816.
Sand, S.E., Donslund, B., 1985. Influence of wave board type on bounded long waves. J. Hydraul. Res. 23, 147–163.
Schäffer, H.A., 1994. The influence of evanescent modes in second order wave generation. Proc. Waves - Physical and Numerical Modelling, Vancouver, B.C., Canada 2, 118–127.
Schäffer, H.A., 1996. Second-order wavemaker theory for irregular waves. Ocean Eng. 23, 47–88.
Spinneken, J., Swan, C., 2009a. Second-order wave maker theory using force-feedback control. Part i: a new theory for regular wave generation. Ocean Eng. 36, 539–548.
Spinneken, J., Swan, C., 2009b. Second-order wave maker theory using force-feedback control. Part ii: an experimental verification of regular wave generation. Ocean Eng. 36, 549–555.
Sriram, V., Schlurmann, T., Schimmels, S., 2015. Focused wave evolution using linear and second order wavemaker theory. Appl. Ocean Res. 53, 279–296.
Taherkhani, M., Vitousek, S., Barnard, P.L., Frazer, N., Anderson, T.R., Fletcher, C.H., 2020. Sea-level rise exponentially increases coastal flood frequency. Sci. Rep. 10, 1–17.
Taylor, P., Williams, B., 2004. Wave statistics for intermediate depth water — NewWaves and symmetry. J. Offshore Mech. Arctic Eng. 126, 54–59.
Tian, Z., Perlin, M., Choi, W., 2011. Frequency spectra evolution of two-dimensional focusing wave groups in finite depth water. J. Fluid Mech. 688, 169.
Tromans, P.S., Anaturk, A.R., Hagemeijer, P., et al., 1991. A New Model for the Kinematics of Large Ocean Waves-Application as a Design Wave.
Ursell, F., Dean, R.G., Yu, Y., 1960. Forced small-amplitude water waves: a comparison of theory and experiment. J. Fluid Mech. 7, 33–52.
Van der Meer, J., Allsop, N., Bruce, T., De Rouck, J., Kortenhaus, A., Pullen, T., Schüttrumpf, H., Troch, P., Zanuttigh, B., 2018. EurOtop: Manual on Wave Overtopping of Sea Defences and Related Structures: an Overtopping Manual Largely Based on European Research, but for Worldwide Application.
Van Leeuwen, P., Klopman, G., 1996. A new method for the generation of second-order random waves. Ocean Eng. 23, 167–192.
Vyzikas, T., Stagonas, D., Buldakov, E., Greaves, D., 2018. The evolution of free and bound waves during dispersive focusing in a numerical and physical flume. Coast Eng. 132, 95–109.
Walker, Daniel AG., T, P.H., Taylor, R.E., 2004. The shape of large surface waves on the open sea and the Draupner new year wave. Appl. Ocean Res. 26, 73–83.
Whittaker, C., Raby, A., Fitzgerald, C., Taylor, P., 2016. The average shape of large waves in the coastal zone. Coast Eng. 114, 253–264.
Whittaker, C.N., Fitzgerald, C.J., Raby, A.C., Taylor, P.H., Orszaghova, J., Borthwick, A. G., 2017. Optimisation of focused wave group runup on a plane beach. Coast Eng. 121 (44), 55.
Whittaker, C., Fitzgerald, C., Raby, A., Taylor, P., Borthwick, A., 2018. Extreme coastal responses using focused wave groups: overtopping and horizontal forces exerted on an inclined seawall. Coast Eng. 140, 292–305.
Young, I.R., Ribal, A., 2019. Multiplatform evaluation of global trends in wind speed and wave height. Science 364, 548–552.